International Journal of Fluid Machinery and Systems
Vol. 8, No. 1, January-March 2015

DOI: http://dx.doi.org/10.5293/IJFMS.2015.8.1.023
ISSN (Online): 1882-9554

Original Paper

Rotordynamic Performance Measurements of An Oil-Free Turbocharger Supported on Gas Foil Bearings and Their Comparisons to Floating Ring Bearings

Yong-Bok Lee[1], Dong-Jin Park[2], and Kyuho Sim[3]

[1]Center for Urban Energy Systems, Korea Institute of Science and Technology, Seoul, Korea, lyb@kist.re.kr
[2]CAE Group, LCD division, Samsung Electronics, Suwon, Korea, dj100.park@samsung.com
[3]Department of Mechanical System Design Engineering, Seoul National University of Science and Technology, Seoul, Korea, khsim@seoultech.ac.kr

Abstract

This paper presents the rotordynamic performance measurement of oil-free turbocharger (TC) supported on gas foil bearings (GFBs) for 2 liter class diesel vehicles and comparison to floating ring bearings (FRBs). Oil-free TC was designed and developed via the rotordynamic analyses using dynamic force coefficients from GFB analyses. The rotordynamics and performance of the oil-free TC was measured up to 85 krpm while being driven by a diesel vehicle engine, and compared to a commercial oil-lubricated TC supported on FRBs. The test results showed that the GFBs increased the rotor speed by ~ 20% at engine speeds of 1,500 rpm and 1,750 rpm, yielding the reduction of turbine input energy by more than 400 W. Incidentally, an external shock test on the oil-free TC casing was conducted at the rotor speed of 60 krpm, and showed a good capability of vibration damping due to the well-known dry friction mechanism of the GFBs.

Keywords: turbocharger, gas foil bearings, floating ring bearings, rotordynamic performance.

1. Introduction

An oil shock that occurred in the 1970s gave diesel engines a higher economic status than gasoline engines, and encouraged their distribution in the market due to their higher economical efficiency and specific power along with the turbocharging technology. Moreover, the current worldwide trend requires more the turbocharging to reduce the size of vehicle engines in response to the energy crisis and stricter regulations for exhaust gas. In order to improve the specific power and increase fuel efficiency, the usage of turbochargers (TCs) has come into even greater demand.

The TC is a turbine-driven compressor. When exhaust gas flows within the turbo housing, turbo wheels are rotated; as the compressor wheel are rotated by the turbine, the external air is compressed and sent to the combustion chamber [1]. TCs, attached to the emission manifold of engines, comprise a turbine wheel, a compressor wheel, a shaft, and bearings. TCs are always exposed to heat owing to a turbine drive that utilizes high-temperature exhaust gas. Therefore, fluid bearings are usually used to achieve lubrication as well as cooling. Fluid bearings support the rotating shaft with a thin oil film; in particular, floating ring oil bearings (FRBs) undergo high vibration attenuation and achieve high-speed stability owing to the pair of oil films inside and outside of the floating ring. Figure 1 (a) shows an image of a TC supported by oil bearings.

Active research is being conducted on TCs to improve their rotordynamic and turbocharging performance through oil lubrication. Currently, turbocharging methods are mostly the two type of waste gate TC (WGT) and variable geometry TC (VGT) [1]. The WGT eliminates exhaust gas to prevent overload when the exhaust gas exceeds the rotation level of the turbine wheels. It controls the amount of exhaust gas that comes into the turbine—in other words, the boost pressure. On the other hand, the VGT differs from a fixed turbo as it controls the angle of the turbine wheel as well as the amount and speed of the exhaust gas. When it is in low-rotation mode, the cross-sectional area of the turbine is decreased so that the dynamic energy of the fluid increases, leading to an increase in the turbine wheel rotation speed. When it is in high-rotation mode, the entrance is extended, so a large amount of exhaust gas comes in to generate a high level of power. However, there is no fundamental resolution yet for turbo lag that causes degradation in the acceleration response and turbocharging performance due to the relatively high inertia of the turbine

Received October 28 2014; revised November 18 2014, December 21 2014; accepted for publication December 21 2014: Review conducted by Prof. Yoshinobu Tsujimoto. (Paper number O14030C)
Corresponding author: Kyuho Sim, Professor, khsim@seoultech.ac.kr

wheel and the high friction of the oil bearing.

Many researchers have attempted to apply gas foil bearings (GFBs) to a TC in order to improve the bearing friction, which strongly influences the acceleration response and turbocharging characteristics at low speed. GFBs use air with very low viscosity as a lubrication medium. Thus, during acceleration, there is minimal delay in the response due to a low friction. Moreover, the oil-free TC is an eco-friendly, compact, and light-weight with minimal power loss. As shown in Fig. 1 (b), the oil-free TC consists of a compressor that provides compressed air, a turbine that produces torque, and a shaft supported by GFBs. For rotor parts, the turbine wheels and compressor wheels are located on both ends, and the shaft is supported by a pair of journal GFBs and a pair of thrust GFBs. GFBs absorb the thermal expansion of the shaft at high temperatures due to the deformation of the foil structure, and improves the damping characteristics by means of the dry friction between the foil and housing [2-4].

GFBs are a type of the hydrodynamic bearings, including one or more foils between the rotor and bearing housing. The geometry of journal GFBs are shown in Fig. 2(a). The top foil forms a soft bearing surface, and the bump foil acts as an elastic foundation under the top foil. The compliance of the bump foil leads to a wider minimal film region, resulting in a higher load capacity and stable operations. This foil structure are also applied to thrust bearings, as shown in Fig. 2(b). Since the mid-1970s, GFBs have been targeted for high-speed and high-temperature rotating machinery in order to prevent instability that occurs during high-speed rotation and to mitigate the influence of heat at high temperatures. They also started being utilized in order to prevent high precision during the processing stage. In 1983, Heshmat et al. [5] were the first to perform a numerical analysis of bump foil bearings. They modeled the bump foil using an elastomeric and compressible Reynolds equation as done for oil films. They then analyzed the load-carrying capacity and bearing friction loss for bump foil bearings. They verified that foil bearings showed a comparatively higher load-carrying capacity than did air bearings. In 1991, Heshmat [6] examined the possibility of applying foil bearings to cryogenic turbopumps of a space shuttle main engine (SSME); in 1993, Heshmat and Hermel [7] experimented with applying foil bearings to an air cycle machine (ACM) that was to be used in commercial aircraft. In 1997, Xiong et al. [8] applied foil bearings to a cryogenic turbo expander and tested it by driving the expander to a maximum rotation speed of 230,000 rpm. For the TC, Howard [9] constructed a rotor design in 1999 to apply a foil bearing to the TC in diesel trucks. In 2000, Heshmat et al. [10] applied foil bearings to a TC with 150 hp and conducted a drive test by raising the speed up to 120,000 rpm on the driving apparatus.

This paper presents the rotordynamic stability and performance measurement of oil-free TC supported on GFBs for 2 liter class diesel vehicles. Oil-free TC was designed and developed via the rotordynamic analyses using dynamic force coefficients from GFBs analyses. The rotordynamics and performance of the oil-free TC was measured up to 85 krpm while being driven by a diesel vehicle engine, and compared to a commercial oil-lubricated TC supported on FRBs.

2. Descriptions of test GFBs and TC

Figure 2 shows a schematic diagram of journal and thrust GFBs for the oil-free TC. The journal GFBs at the turbine and compressor sides have a length of 20.4 mm, and an identical bearing configuration. The top and bump foils are spot-welded at one end on the inner surface of the bearing housing and are free at the other end. The thrust GFBs have four bearings pads, each of which has a single top foil and a single bump foil with bump geometry identical to that of the journal GFBs. The arc length of the inclined plane is 40 degrees. Incidentally, the control pin connected to a hydraulic actuator maneuvers the turbine nozzle area for flow rate control of the exhaust gas. Table 1 details the geometry and material of the journal and thrust GFBs for the oil-free TC.

Figure 3 shows a drawing of oil-free TC supported on GFBs. The TC rotor with a diameter of 24 mm contains turbine and compressor impellers at each end and a thrust collar located between them, closer to the compressor. Nuts are used to assemble the impellers to the rotor, and the nut located on the compressor side has a polished surface for measurement of the lateral rotor motions. The total mass and length of the rotor are 0.31 kg and 108 mm, respectively. The shaft is made from Inconel 718 and is coated with a wear-resistant solid lubricant, CORONA 910 [14] of thickness 0.25 mm for reduction of wear and friction at high temperatures and during start/stop. Table 2 presents the geometry and material of the oil-free TC supported on GFBs.

Table 1 Geometry and materials of GFBs.

Part	Unit	Value
Journal Bearing	Diameter	24.0 mm
	Top foil thickness	0.12 mm
	Bump foil thickness	0.12 mm
	Length (turbine side)	20.4 mm
	Length (compressor side)	20.4 mm
	Material	Inconel X750
Thrust Bearing	Outer diameter	49 mm
	Inner diameter	25 mm
	Thickness of top and bump foil	0.12 mm
	Number of top foil pad	4
	Inclined angle	40 deg
	Material	Inconel X750

Table 2 Geometry and materials of oil-free TC supported on GFBs.

Shaft	Length	108 mm
	Mass	0.31 kg
	Diameter	24.0 mm
	Material	Inconel 718
Compressor impeller	Mass	0.018 kg
	Polar inertia	2.67 x 10^{-6} Kg-m^2
	Max. efficiency	78 %
	Material	Al alloy
Turbine impeller	Polar inertia	4.33 x 10^{-6} Kg-m^2
	Mass	0.042 kg
	Max. efficiency	56 %
	Material	Inconel 718

3. Rotordynamic Analysis of oil-free TC

A rotor dynamics analysis of the oil-free TC supported on GFBs is conducted with a finite element model of the TC based on dynamic force coefficients of the GFBs. The journal GFBs are assumed as a linear spring-damper with two degrees of freedom. The dynamic force coefficients of the journal GFBs are calculated from a perturbation analysis at a given excitation frequency around a static equilibrium position. In the analysis, the shaft is perturbed harmonically with an infinitesimal amplitude, and the perturbed shaft also induces perturbed motions of the top and bump foils. The equilibrium position is searched using the Newton-Raphson method, wherein the pressure field in the air film is calculated by solving the Reynolds equation, Eq. (1), at each iteration. Details of the perturbation analysis of GFBs can be found elsewhere [11–13].

In general, the bump foil is modeled as a simple elastic foundation with stiffness and damping [5]; however, in this study, the finite element method was applied to the bump foil for structural analysis and coupled with fluid film flow analysis [12]. The Reynolds equation for a compressible fluid flow in the film region is given as:

$$\frac{\partial}{\partial x}\left(ph^3 \frac{\partial p}{\partial x} \right) + \frac{\partial}{\partial z}\left(ph^3 \frac{\partial p}{\partial z} \right) = 6\mu\Omega R \frac{\partial}{\partial x}(ph) + 12\mu \frac{\partial}{\partial t}(ph) \tag{1}$$

where p is the hydrodynamic pressure of the air film flow, h is the film thickness, μ is the dynamic viscosity of the air, R is the bearing radius, and Ω is the angular speed of the shaft. (x,z) are the circumferential and axial coordinates on the plane of the bearing. The Reynolds equation is solved with the boundary conditions for the ambient pressure at all of the side edges and the leading and trailing edges. The film thickness for a perfectly aligned journal is

$$h = C + e_X \cos\theta + e_Y \sin\theta - r_p \cos(\theta - \theta_p) + w_d \tag{2}$$

where e_X and e_Y are the journal eccentricity in the inertial axes, X and Y, w_d is the local bump deflection, r_p is the mechanical preload, C is the nominal bearing clearance, and θp is the pivot angle of each lobe. The local bump deflection depends on the bump structural stiffness of the elastic foundation and the film pressure.

Figure 4 shows the stiffness and damping coefficients of the GFBs for the oil-free TC over the rotor speeds. The direct stiffness coefficients (K_{xx}, K_{yy}) gradually increased with rotor speed, while the difference between the cross-couple stiffness (K_{xy}-K_{yx}) clearly decreased, which is known to cause the rotordynamic instability. All the damping coefficients greatly reduced at higher speeds, showing a typical characteristic of air bearings.

The rotordynamic model of TCs supported by GFBs has 29 beam elements for the shaft in the TC and three disk elements (thrust collar, turbine wheel, and compressor wheel), and two bearing elements. Figure 5 shows the Finite element model of oil-free TC rotor with turine and compressor impellers and GFBs. The rotordynamic analysis results showed that in terms of rigid body vibration, the critical speeds of the conical and cylindrical modes were 3,000 rpm and 11,500 rpm, respectively, which are far below the TC speed, approximately 25,000 rpm, at engine idle. The critical speed for the first bending mode was 197,600 rpm, which is above a maximum TC operating speed. The predicted bending critical speed agrees well with the measured one from the impact test, which is approximately 205, 000 rpm.

4. Experimental Results

Figure 6 shows the manufactured test TC supported on GFBs. The compressor impeller and turbine wheel along with their housings were reused from a commercial variable-geometry TC supported on FRBs. Figure 7 also shows the TC experimental equipment driven by a 2.2 L Santafe diesel engine under the condition of free running (no torque); the TC compressor and turbine inlet/outlet were connected to the diesel engine through extension pipes. The TC was installed on a vibration table to inflict external shock. A tachometer was used to measure the speed of the engine crankshaft and TC shaft. An accelerometer and displacement sensor measure the TC housing vibration and rotor motion, respectively.

The rotordynamic and turbocharging performances of the oil-free TC presented above were compared with those of the commercial FRB TC by using the experimental equipment driven by the diesel engine. Figure 8 shows the TC and engine speeds

versus time for FRBs and GFBs, driven by the diesel engine. In the idle state of about 900 rpm, both TCs rotated at low speeds between 5000 and 10,000 rpm; when the engine accelerated, the rotation speeds increased. At an engine rotating speed of 1,500 rpm, the rotation speeds of TC with the FRBs and GFBs were 60,000 and 72,000 rpm, respectively. When the engine rotation speed was 1,750 rpm, the two TCs rotated at speeds of 62,000 and 80,000 rpm, respectively. As a result, the TC's rotation speed increased by about 20% owing to the GFB application. This result indicates the low-friction quality of the GFB; the increase in rotation speed directly enhanced the outlet pressure of the compressor impeller, and therefore improve the turbocharging performance.

Figure 9 shows the turbine inlet pressure and the rotor speed versus engine speed for TCs supported by FRBs and GFBs. The turbine inlet pressure increases from 1.1 bar to 1.7 bar as the engine speed increases from 900 rpm to 2,400 rpm. The TC supported by the GFBs requires a lower engine speed than that supported by the FRBs, indicating low friction loss of the bearings. The difference in the engine speeds greatly increases at higher engine speeds. The following equation calculates the input power of the TC from the estimated flow of the turbine inlet pressure and engine speed.

$$P_{in} = \boldsymbol{m} c_p T_{in} = c_p p_{in} Q_{in} / R_g \tag{1}$$

where P_{in} is the input power to TC, $\boldsymbol{m}$ is the exhaust mass flow rate into turbine, c_p is the specific heat under constant pressure, and R_g is the gas constant. T_{in}, p_{in}, and Q_{in} are the exhaust gas temperature, pressure, and volume flow rate, respectively. The volume flow rate is the product of the engine volumetric capacity and the engine speed. The TC input power is calculated with the inlet pressure in Fig. 9(a) and the calculated volume flow rate of the exhaust gas. At the TC speed of 72,000 rpm, the engine speeds for GFBs and FRBs are approximately 1,400 rpm and 2,100 rpm, respectively. The engine speed difference produces a decrease in the TC input power, 462 W, which mainly results from the reduction in the bearing friction. At the TC speed of 85,000 rpm, the reduction in the TC input power is 420 W. Note that the reduction in the TC input power is observed at TC speeds below 50,000 rpm; however, it rapidly increases at higher TC speeds.

Figure 10 shows the rotor lateral responses measured at the compressor end for FRBs and GFBs at a TC speed of 80,000 rpm, driven by the diesel engine. For the FRBs, the rotor motion appears to have high-level sub-synchronous vibration components, mainly because of the hydrodynamic instability due to the oil lubrication. On the other hand, GFBs shows a low-frequency sub-synchronous component generated by the engine vibration of 50 Hz; however, it is relatively sinusoidal vibration with dominant synchronous component, demonstrating stable rotordynamic operations.

Figure 11 shows the time responses of rotor vibration and isolator acceleration upon impact force applied on the casing of TC supported by GFBs at the rotor speed of 60,000 rpm, driven by the diesel engine. As shown in Fig. 11(a), the pneumatic vibration table that isolates the TC from the ground showed a small vibration amplitude due to the transfer of the engine vibration. When an external impact load of 400 N was applied, a maximum shock vibration of 0.36 *g* occurred. The vibration table quickly absorbed the applied shock vibration in about 0.05 s, thus showing an effective transfer of the impact onto the TC. The TC rotor vibrated at an amplitude of about 4 μm in a normal state. When an external shock of 0.36 *g* was applied to the TC casing, a maximum shock vibration of the TC rotor reached 4 μm and quickly attenuated within 0.25 s. This results confirms that GFBs can effectively absorb external shocks that occur because of energy-dissipative friction motions between the bump foil and the mating surfaces. In addition, the TC supported on GFBs operated in a stable manner even with periodic engine vibrations.

5. Conclusions

This study examined the rotordynamic and turbocharging performance of an oil-free TC supported by GFBs for a diesel vehicle. The rotor-bearing system of a test oil-free TC was designed based on the rotordynamic analysis using the dynamic force coefficients of GFBs. A test bench was configured for the test TC to operate using exhaust gas of a diesel vehicle engine. A comparison of a commercial FRB TC with the foil bearing TC showed that the TC supported by foil bearings provided a 20% higher rotation speed than that supported by FRBs. This showed that the friction loss of foil bearings is significantly low; moreover, the approximate turbine input energy decreased by over 400 W.

The TC rotor vibrations for the GFB and FRB were compared at an TC speed of 80,000 rpm. The FRBs were dominated by asynchronous components, but the GFBs showed sinusoidal characteristics that were dominated by the synchronous component. An external shock test was conducted with an impact load applied on the casing of a TC with foil bearings at a rotor speed of 60,000 rpm. The result showed that the bump foil structure of the foil bearing effectively attenuated a large rotor vibration caused by the external shock.

In conclusion, the oil-free TC supported by foil bearings showed improvements in rotordynamic and turbocharging performance. Furthermore, the vibration damping ability of the GFBs against external shock demonstrates a possible use of the oil-free TC for real vehicle engines.

Acknowledgements

This material is based on work supported by the Korea Institute of Science and Technology (KIST) Research Projects: R&D on Power Generation and Energy Storage Technology for Tri-Gen Systems.

Nomenclature

c_p : specific heat at constant pressure [J/kg-K]
D : bearing damping coefficient [N-s/m]
h : film thickness [m]
K : bearing stiffness coefficient [N/m]

$\boldsymbol{m}$: mass flow rate [kg/s]
p : hydrodynamic pressure of the air film flow [N/m^2]
p_{in} : pressure [N/m^2]
P_{in} : TC input power [W]
Q_{in} : volumetric flow rate [m^3/s]
R : bearing radius [m]
T_{in} : temperature [°C]
η : efficiency
μ : dynamic viscosity of the air [N-m/s]
γ : specific heat ratio
Ω : angular speed of the shaft [rad/s]
ω_n : natural frequency [rad/s]

Subscripts

In, out :Inlet and outlet
X, Y : Global coordinates

References

[1] F. P. Miller, 2009, Turbocharger, Alphascript Publishing.
[2] C. DellaCorte, V. Lukaszewicz, M. J. Valco, K. C. Radil, and H. Heshmat, 2000, "Performance and Durability of High Temperature Foil Air Bearings for Oil-Free Turbomachinery," STLE Tribology Transactions, 43(4) 774-780.
[3] K. Radil, S. Howard, and B. Dykas, 2002, "The Role of Radial Clearance on the Performance of Foil Air Bearings," STLE Tribology Transactions, 44(4), pp. 485-490.
[4] C. DellaCorte, and M. J. Valco, 2000, "Load Capacity Estimation of Foil Air Journal Bearings for Oil-Free Turbomachinery Applications," Proceedings fo ASME/STLE Joint Tribology Conference, 00-TC-4.
[5] H. Heshmat, J. A. Walowit, and O. Pinkus, 1983 "Analysis of Gas-Lubricated Foil Journal Bearings," ASME Journal of Lubrication Technology, 105 pp. 647-655.
[6] H. Heshmat, 1991, "A Feasibility Study on the Use of Foil Bearings in Cyrogenic Turbopumps," AIAA, Paper No. AIAA-91-2103-CP.
[7] H. Heshmat, and O. Hermel, 1993, "Compliant Foil Bearing Technology and Their Application to High Speed Turbomachinery," The 19th Leeds-Lyon Symposium on Thin Film in Tribology, pp. 559-575.
[8] L. –Y. Xiong, G. Wu, Y. Hou, L. –Q. Liu, M. –F. Ling, and C. –Z. Chen, 1997, "Development of Aerodynamic Foil Journal Bearings for a High Speed Cryogenic Turboexpander," Cryogenics, 37 221-227.
[9] S. A. Howard, "Rotordynamics and Design Methods of An Oil-free Turbocharger," NASA/CR-1999-208689.
[10] H. Heshmat, J. F. Walton, C. Dellacorte, and M. Valco, 2000, "Oil-free Turbocharger Demonstration Paves Way to Gas Turbine engine Applications," Proceedings of the ASME Turbo Expo, ASME 2000-GT-620.
[11] T. H. Kim, and L. San Andres, 2008, "Heavily Loaded Gas Foil Bearings: A Model Anchored to Test Data," ASME Journal of Engneering for Gas Turbines and Power, 130 (1) , 012504.
[12] D. J. Park, C. H. Kim, G. H. Jang, and Y. B. Lee, 2008, "Theoretical considerations of static and dynamic characteristics of air foil thrust bearing with tilt and slip flow," Tribology International, Vol. 41, No. 4, pp. 282-295.
[13] N. S. Lee, 2003, A Study on the Performance and Stability of Air Bump Foil Bearing, PhD Thesis, Hanyang University.
[14] Y.-B. Lee, D.-J. Park, J. H. Jo, and C. H. Kim, 2007, "High Temperature Lubricants for Air Foil Bearings: Friction and Wear Characteristics of Corona Series from 25 to 1,000 °C," Proceedings of STLE Annual Meeting, Philadelphia, USA.

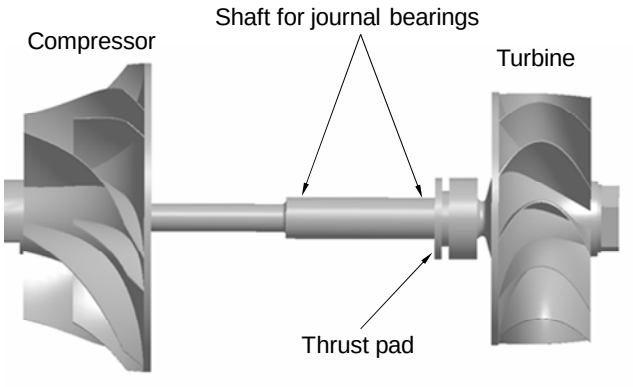

(a) TC rotor for FRBs

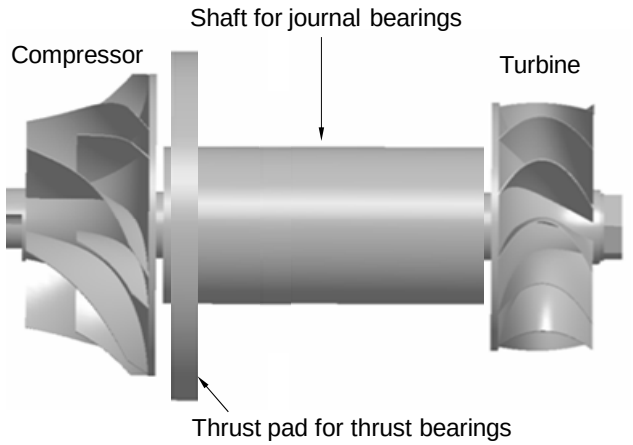

(b) TC rotor for GFBs

Fig. 1 Configurations of TC rotors for (a) FRBs and (b) GFBs.

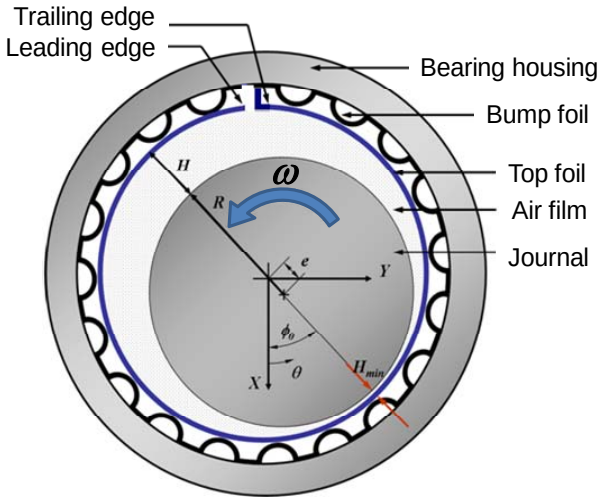

(a) Journal GFB

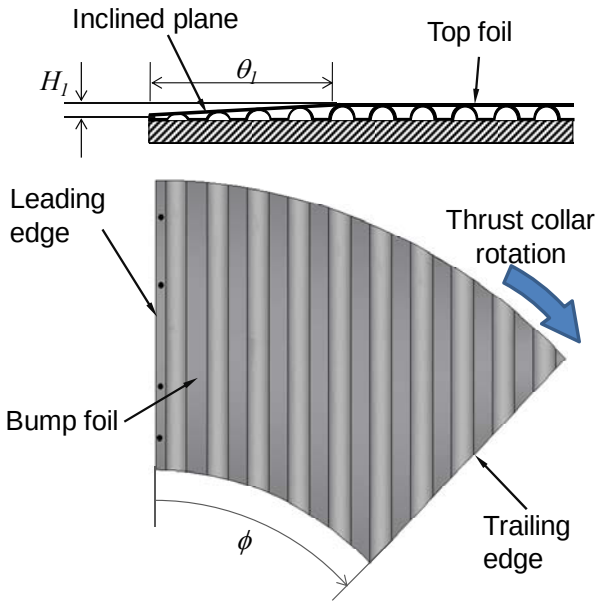

(b) Thrust GFB

Fig. 2 Schematic of journal and thrust GFBs for the oil-free TC.

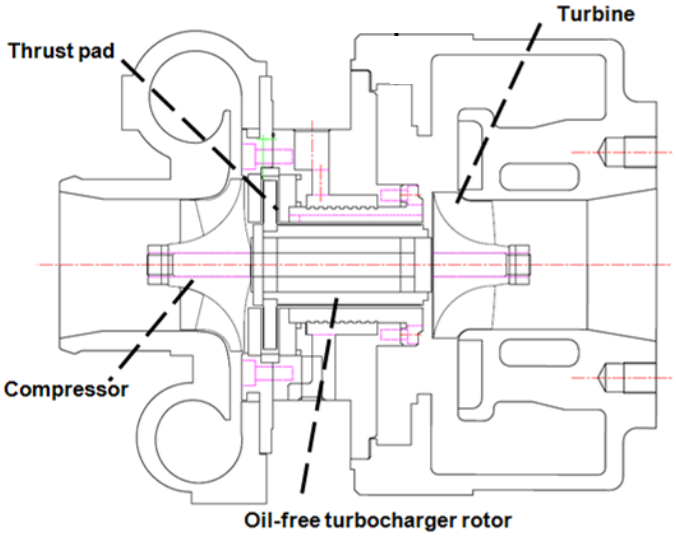

Fig. 3 Drawing of oil-free TC supported on GFBs.

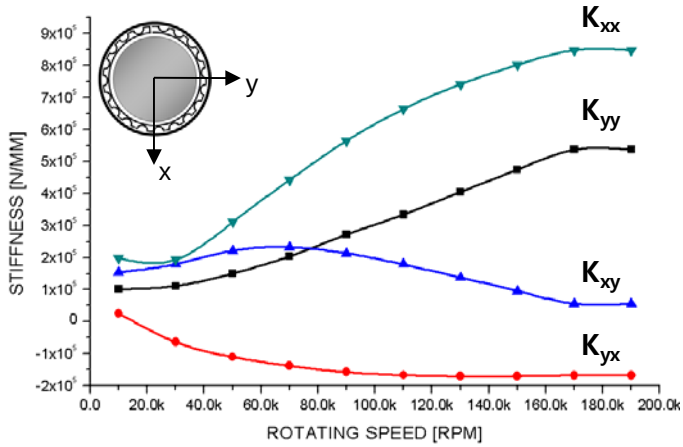

(a) Stiffness coefficient

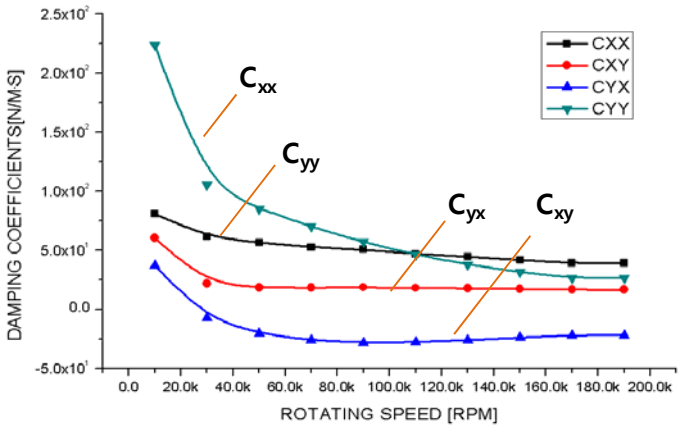

(b) Damping coefficient

Fig. 4 Dynamic force coefficient of GFBs from bearing analysis.

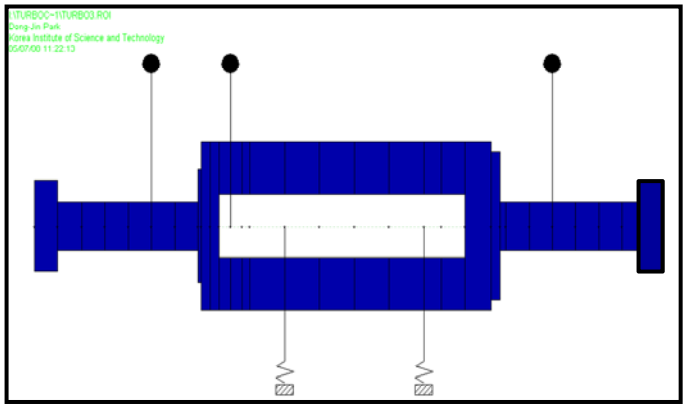

Fig. 5 Finite element model of oil-free TC rotor supported on GFBs.

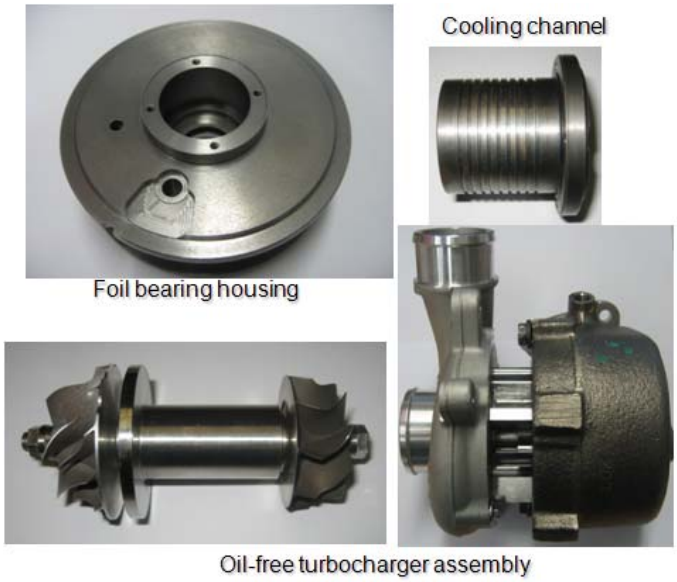

Fig. 6 Manufactured oil-free TC with the assembly of rotor and housing.

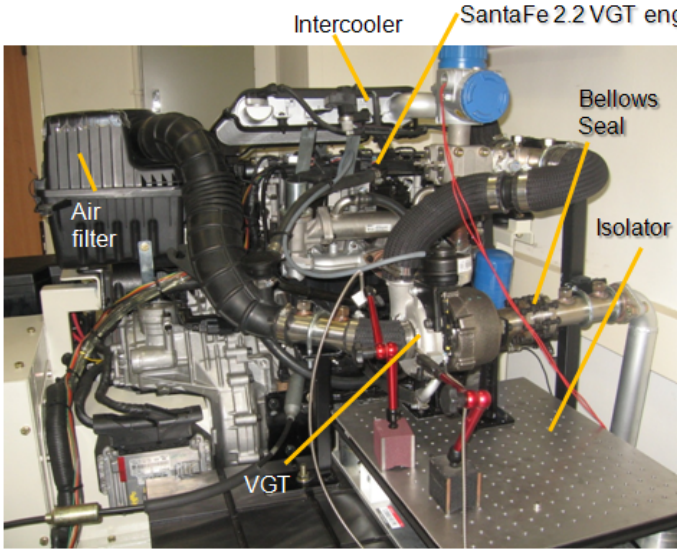

Fig. 7 Test bench for oil-free TC driven by a diesel vehicle engine for Santafe 2.2L.

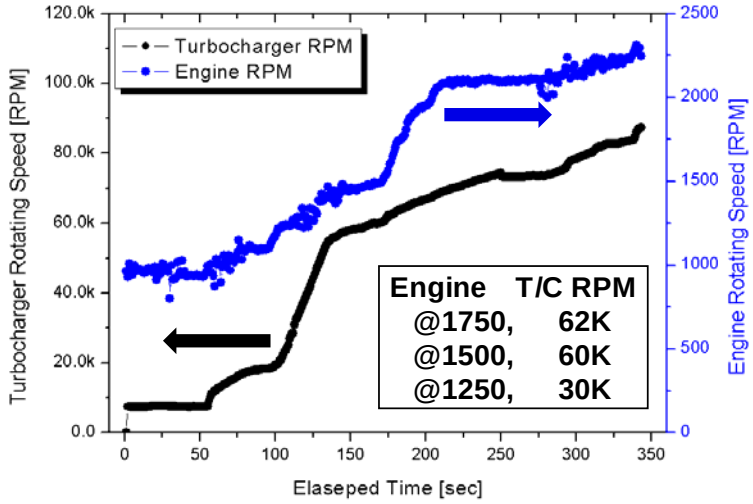

(a) FRBs

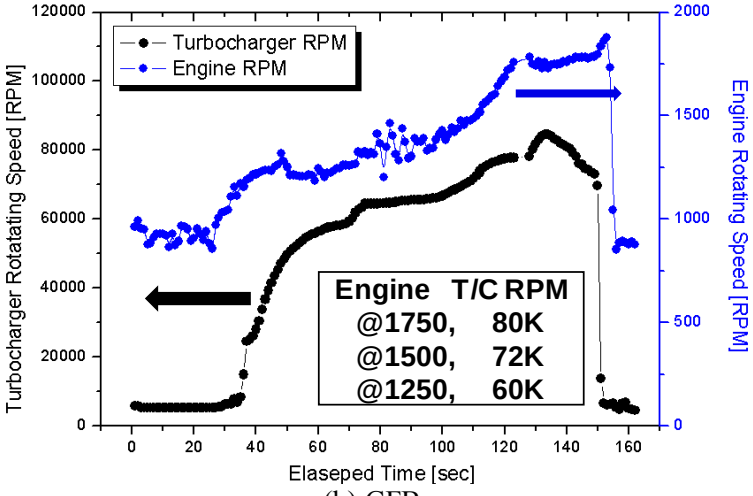

(b) GFBs

Fig. 8 Rotor speed of TC supported on floating ring bearings and GFBs, driven by a diesel engine.

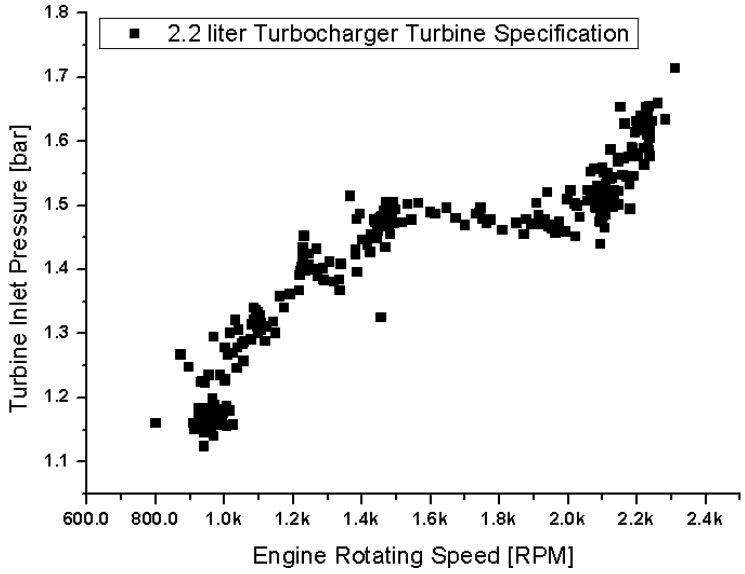

(a) Turbine inlet pressure for FRBs

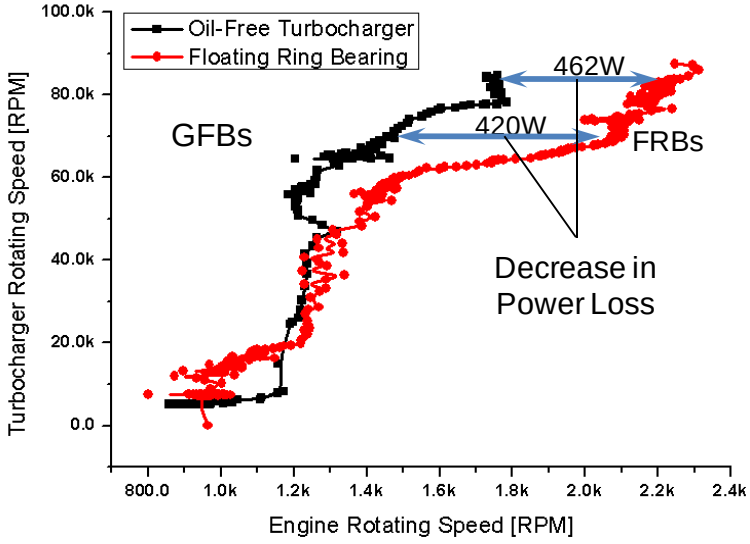

(b) TC rotor speed for FRBs and GFBs

Fig. 9 TC performance from compressor exit pressure and rotor speeds, driven by a diesel engine.

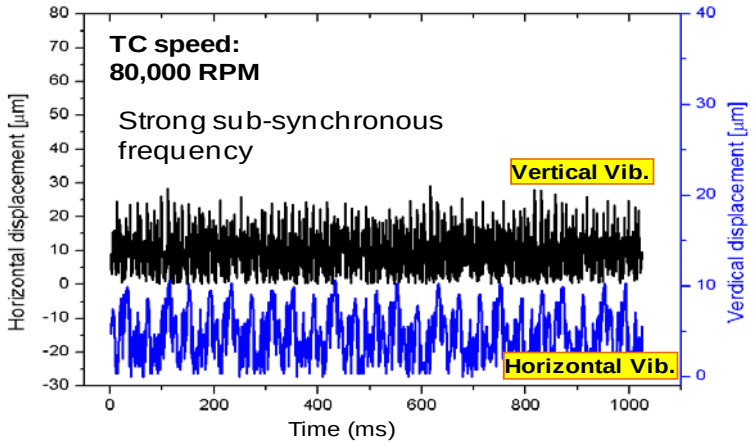

(a) FRBs

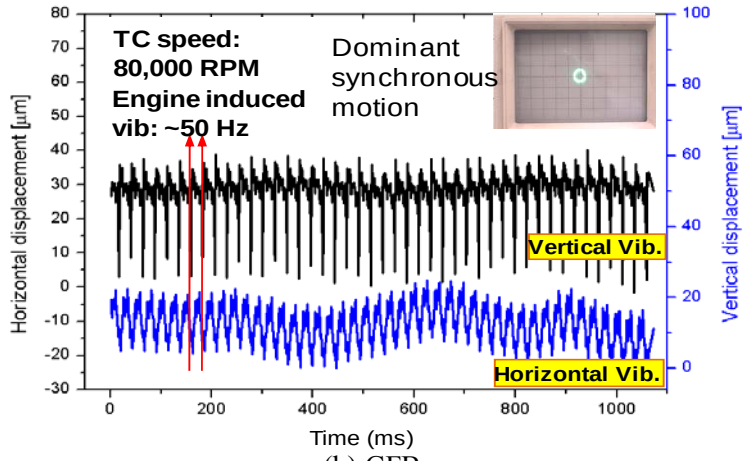

(b) GFBs

Fig. 10 Rotor lateral responses at compressor end for floating ring bearings and GFBs, driven by a diesel engine.

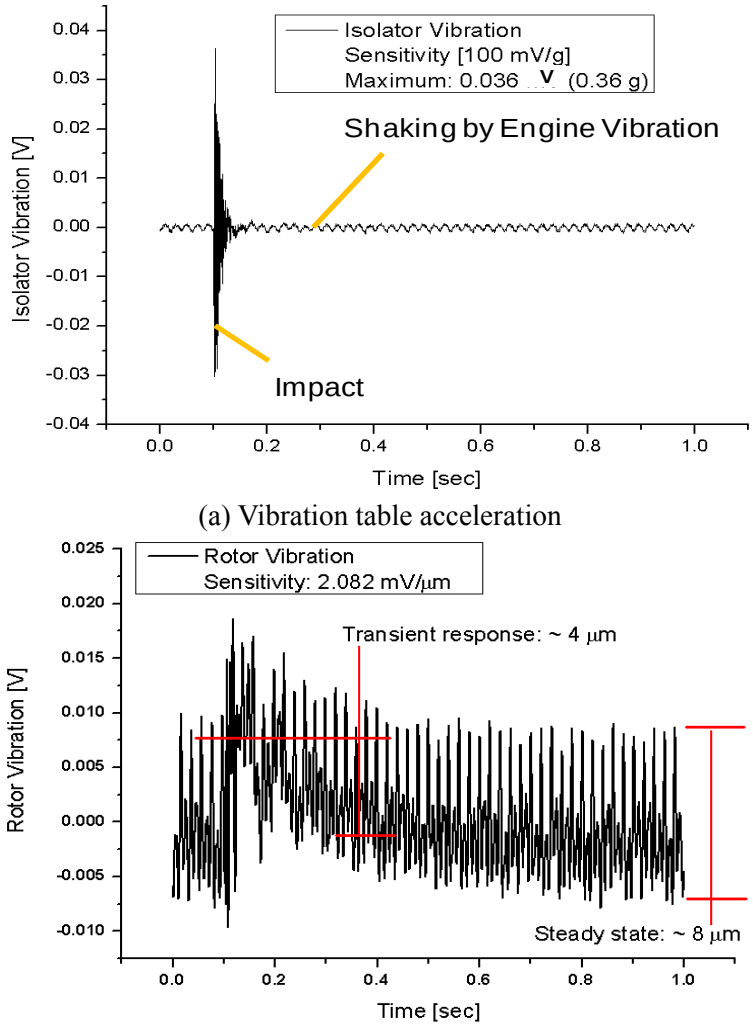

(a) Vibration table acceleration

(b) Rotor vibration, rotating at 60,000 rpm

Fig. 11 Time responses of rotor vibration and isolator acceleration upon impact force applied on the casing of TC driven at 60,000 rpm.